Paleoclimatic Signature in Terrestrial Flood Deposits

Christine E. Koltermann and Steven M. Gorelick

Large-scale process simulation was used to reconstruct the geologic evolution during the past 600,000 years of an alluvial fan in northern California. In order to reproduce the sedimentary record, the simulation accounted for the dynamics of river flooding, sedimentation, subsidence, land movement that resulted from faulting, and sea level changes. Paleoclimatic trends induced fluctuations in stream flows and dominated the development of the sedimentary deposits. The process simulation approach serves as a quantitative means to explore the genesis of sedimentary architecture and its link to past climatic conditions and fault motion.

The record of terrestrial deposition and erosion represents a synthesis of geologic, hydrologic, and climatic processes. Key influences include large-scale structural evolution, sea level changes, and climatic variation that has driven the history of catastrophic floods and droughts. Many of these processes can now be mathematically described. Equations that govern fluid flow and sediment transport are solvable with the use of large-scale mathematical simulations.

In this article, we present the results of a three-dimensional numerical reconstruction of the Alameda Creek alluvial fan in north central California. This fan deposit is of interest because it lies in a near-coastal environment that has remained active tectonically during the late Quaternary, and local climate varied significantly throughout this period. Genesis of the fan has not been explained previously, even though there are numerous deep wells that constrain possible paleoreconstructions. Through simulation, we evaluated the complex interactions of geologic and hydrologic processes that produced the fan deposit.

Representing Sedimentary Architecture

Three types of models have been used to mimic patterns in sedimentary deposits: descriptive, structure-imitating, and process-imitating. Descriptive models classify depositional environments, facies relations, and sedimentary basins (*1*). Although extremely useful tools for interpretation, descriptive models cannot be used to quantitatively test hypotheses regarding detailed geologic history. Structure-imitating models are aimed at the reproduction of geometric relations of sedimentary deposits. One class of structure-imitating models, sequence stratigraphy, relies on empirical relations among rates of sea level change, subsidence, and sedimentation to develop cross sections of deposits (*2*). Another class of structure-imitating models relies on spatial statistics and probabilistic rules to generate geometric patterns similar to those seen in nature (*3*). A related approach combines limited process-based simulation with structure imitation (*4*). Models that do not consider the mechanisms by which sedimentary deposits form provide little understanding of geologic environments and may lead to interpretations that are geologically impossible.

Sedimentary process simulation allows one to interpret paleoenvironments through quantitative study. In process models, physical mechanisms are formulated in terms of governing partial differential equations (*5*,

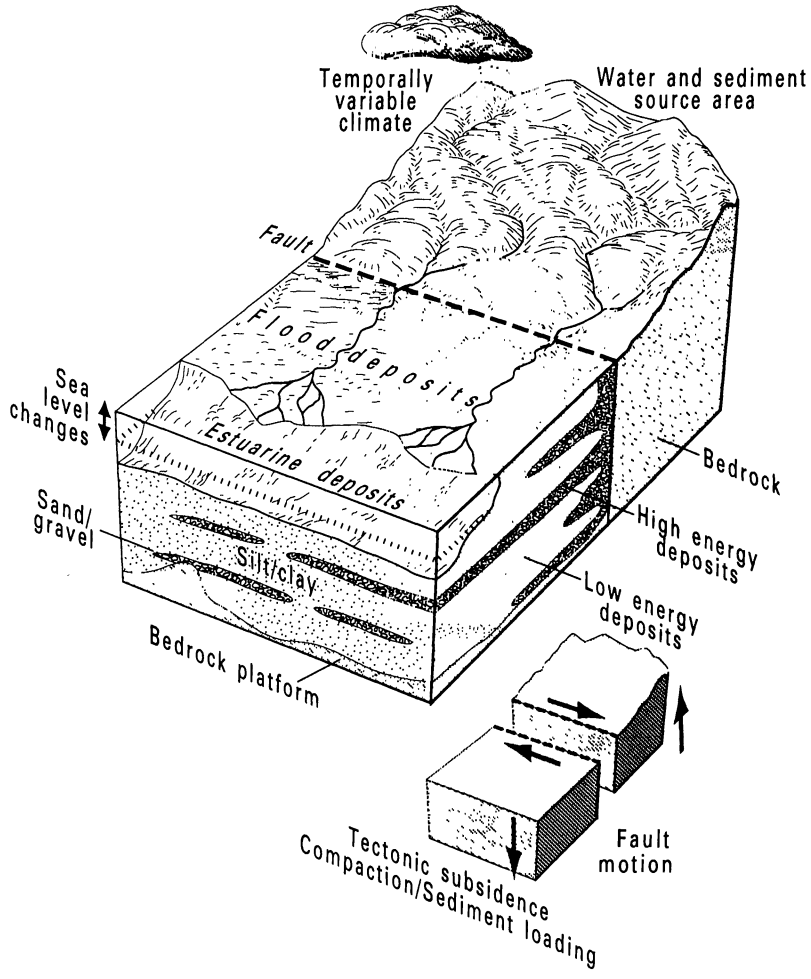

Fig. 1. Conceptualization of physical processes. In our model, we account for the interactions of climate variability, flooding, sedimentation, erosion, tectonics, subsidence, and sea level change.

The authors are in the Department of Applied Earth Sciences, Stanford University, Stanford, CA 94305.

6). This approach depicts interactions of geologic processes operating over different spatial and temporal scales. Thus, it produces an integrated representation of the geology. Our simulation of geologic evolution builds upon previous work in its consideration of important external forces that influence sedimentation. These forces include variations in climate, land movements, and sea level change.

The Sedimentary Process Model

This dynamic model produces three-dimensional reconstructions of sedimentary deposits that formed over hundreds of thousands of years. The model was made on the basis of several principles: conservation of mass and momentum for fluid, a flow resistance equation, conservation of mass for sediment, a relation between the rate of erosion or deposition and the size distribution of sediments transported, and a relation describing changes in topography resulting from erosion or deposition. An earlier model of the physics of fluid flow included empirical relations for sediment transport (5). This model was extensively modified to represent depositional processes more precisely. We added explicit process descriptions of relative sea level change, tectonics, subsidence, compaction, variable sediment porosity, paleoclimate-driven fluctuations in floods and sediment loads, and stochastic generation of streamflow time series (Fig. 1). The model was then adapted to large-scale supercomputer use.

Fluid flow model. A complete account of unsteady fluid flow in three dimensions is provided by the mass conservation and the Navier-Stokes force-momentum equations (7). Solving the Navier-Stokes equations in three dimensions for an arbitrary geometry, over geologic time frames, is computationally intractable. With a few simplifying assumptions, however, realistic large-scale problems can be tackled with the use of a supercomputer. The full equations were simplified by a consideration of the flow velocity variations only in the horizontal dimension (5). This approach yielded a two-dimensional, depth-averaged flow model (Table 1). In addition, we simulated fluid flow beneath the sea by accounting for density differences between sediment-laden freshwater and seawater (8).

Our simulations are time-dependent; that is, flow is affected by flood magnitude and velocity as well as erosional and depositional changes in topography. Although the governing equations were solved on a two-dimensional grid of surface topography, the model-generated sedimentary deposit was stored in three dimensions.

Alluvial fan deposits are commonly formed by episodic floods (9). A stochastic streamflow generator, based on a Markov model accounting for lag-one serial correlation, was developed to mimic daily flow sequences occurring in natural streams (10). We assumed that daily flows depend on seasonal flow statistics, daily serial correlation, and a component of random noise. The simulated streamflows represent the natural variability associated with storms and rainfall patterns. Flood generation is the only part of the model containing a random component.

Not all streamflows contribute significantly to fan development. To decide which flood events to simulate, we performed an a priori analysis to determine the amount of sediment transported by different magnitudes of streamflow. An increase in flow will increase the capacity for erosional work needed to move sediment out of a drainage basin (11). For the highly skewed streamflow distributions often found in nature, most of the sediment is transported by just a few large flows. In this study, only those flows greater than five to ten times the arithmetic mean of daily flows were critical in representing the paleohydrologic response. Of the model-generated daily flows representing the passage of 600,000 years, approximately one million daily flood events were selected for simulation, an average of one to two per year.

Sediment transport and consolidation model. Sediment erosion, transport, and deposition respond to the topography and physical properties of both fluid and sediment. Many researchers have recognized that sediment transport is a function of the boundary shear stress (12). Threshold conditions for particle erosion are related to the critical shear stress and particle characteristics (13, 14). These relations led to the empirical sediment transport formula used here (5) (Table 1).

Superimposed on the depositional and erosional response to each flood are horizontal and vertical land block movements caused by tectonics and subsidence. Horizontal displacement, caused by faulting, was tracked with the use of dynamic mesh translation. Vertical displacements were accounted for through continual topographic adjustments dictated by tectonic subsidence, sediment loading, and compaction. The crustal response to sediment loading was calculated by a simple Airy isostatic model (15), which assumes that the earth's crust remains in isostatic equilibrium and that the sediment load on the crust is entirely compensated at the locus of the load. Compaction is computed with porosity versus depth functions for different sediment types (16).

Process-based geologic reconstruction is a large-scale computational problem. We simulated an area of 240 km^2 with a horizontal resolution of 120 m and a vertical resolution of tens of centimeters for 600 layers. Daily flood events were simulated

Table 1. Equations of fluid flow and sediment transport. M, mass; L, length; T, time.

EQUATIONS:

2-D conservation of mass and momentum (5):

$$\frac{\partial h}{\partial t} + \nabla \cdot (h\,\mathbf{Q}) = 0$$

$$\frac{\partial \mathbf{Q}}{\partial t} + (\mathbf{Q} \cdot \nabla)\,\mathbf{Q} = -g\nabla H + \frac{c_2}{\rho}\nabla^2\mathbf{Q} - c_1\frac{\mathbf{Q}\,|\mathbf{Q}|}{h}$$

$$c_1 = \frac{gn^2}{h^{1/3}}$$

Sediment transport (5):

$$V = \left[\frac{c_T\,\tau_o\,Q}{h}\right]$$

$$\tau_o = c_1 Q^2 \rho$$

$$V_e = \sum_{i=1}^{NG} \frac{V_{ei}\,w_i}{c_f}$$

If $V_e > V$ and $\tau_o < \tau_{ci}$, deposit grain size i as a function of [(V_e-V), w_i, Δt, h, D_V]

If $V_e < V$ and $\tau_o > \tau_{ci}$, erode grain size i as a function of [(V-V_e), w_i, Δt, h, D_V]

If $V_e = V$, sediment is transported during Δt

CALIBRATED PARAMETERS:

1) Subaerial roughness coefficient (n).
2) Transport capacity coefficient (c_T).
3) Sediment transportability coefficient (c_f).
4) Subaqueous roughness coefficient (n).
5) Rate of horizontal fault motion.
6) Height of sea level 125,000 years ago.

LIST OF SYMBOLS:

c_1	effective bottom friction coefficient [-]
c_T	transport capacity coefficient [T^{3}L/M]
c_f	sediment transportability coefficient [T/L]
c_2	lateral friction coefficient [M/LT]
D_V	fluid volume [L^3]
g	gravitational acceleration [L/T^2]
h	fluid depth [L]
H	fluid elevation [L]
n	roughness coefficient [T/L$^{1/3}$]
NG	number of grain size classes = 4
Q	depth-averaged horizontal flow velocity [L/T]
Q	vector of Q (x and y components) [L/T]
|**Q**|	the absolute value of **Q** [L/T]
V	sediment transport capacity per unit volume of fluid [-]
V_e	effective sediment volume in transport per unit volume of fluid [-]
V_{ei}	volume of grain size i in transport per unit volume of fluid [-]
w_i	fall velocity of grain size i [L/T]
x, y	spatial coordinates [L]
Δt	time step [T]
ρ	fluid density [M/L^3]
τ_o	boundary shear stress [M/T^{2}L]
τ_{ci}	critical shear stress for grain size i [M/T^{2}L]
∇	spatial derivative operator, $\frac{\partial}{\partial x}, \frac{\partial}{\partial y}$

ASSUMPTIONS FOR 2-D MODEL:

1) Horizontal flow velocity variations only.
2) Hydrostatic conditions.
3) Fluid is homogeneous, isothermal, and incompressible.
4) Coriolis forces are neglected.
5) Bottom friction is described by the semi-empirical Manning equation.
6) The channel bottom is 'rigid' during Δt.

with time steps as small as 5 to 60 s. This simulation required a supercomputer and code vectorization and used approximately 250 central processing unit (CPU) hours on an IBM 3090-600J mainframe; calibration required more than 1200 CPU hours on an HP-DN10000 computer.

Field Environment

The field area provided a comprehensive test of the process model and enabled us to explore the genesis of the sedimentary architecture. Alameda Creek is in north central California, 48 km southeast of San Francisco and bordering San Francisco Bay (Fig. 2). Episodic floods have distributed gravel, sand, silt, and clay in a characteristic fan shape (9). The drainage basin in the Diablo Range is ten times the size of the alluvial fan, which began to form 600,000 years ago, during the last major deformation of the Diablo Range in central California (17).

Four important physiographic features have affected fan deposition: the Diablo Range, the Hayward fault, the Coyote Hills, and San Francisco Bay (Fig. 2). The Diablo Range is the source of fan sediments and is composed of Mesozoic and Tertiary shales and sandstones, as well as Quaternary gravels and sands (18). The Hayward fault is part of the San Andreas fault system, the boundary between the North American and the Pacific plates. The fault, which cuts across the apex of the fan, has right-lateral, strike-slip motion and some vertical offset. Protruding through the unconsolidated fan deposits are the Coyote Hills. They consist of fault-bounded Mesozoic rocks that formed a boundary to deposition during fan development. The effect of San Francisco Bay on deposition has been episodic. During low stands of relative sea level, San Francisco Bay was absent and a northwesterly trending stream valley formed, whereas during high stands of sea level an estuary formed. The influence of sea level variation produced only minor changes in the stream gradient (19).

We resolved the complex fan stratigraphy (shown in two cross sections) (Fig. 3, A and B) on the basis of 63 lithologic logs from water wells and bridge borings (19–22). Continued subsidence provided an ever deepening trap for Alameda Creek sediments; as a result, the Coyote Hills were gradually buried. Subsidence has been so rapid and continuous that marsh plains, rather than deltas, have formed in San Francisco Bay (23). The fan is composed of cycles of coarse (gravel and sand) and fine (silt and clay) deposits that form extensive layers. Similar cycles occur in sediments adjacent to the fan and throughout the San Francisco Bay area (20, 24, 25). The widespread correlation of these cycles suggests at

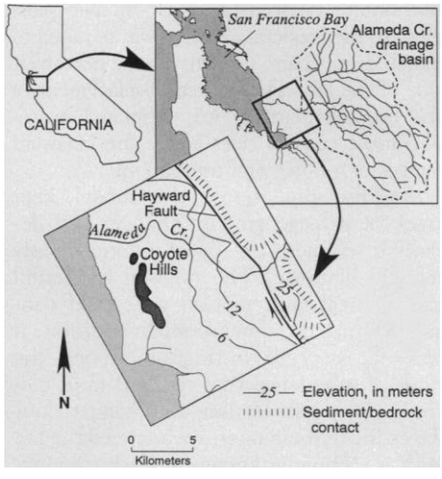

Fig. 2. Location map. The Alameda Creek fan is in the central California Coast Ranges. Alameda Creek flows westerly from the Diablo Range toward San Francisco Bay. The fan covers an area of 170 km^2, and its source area in the Diablo Range mountains is approximately ten times this size. The Hayward fault has remained active during the past 600,000 years. Right-lateral, strike-slip motion has shifted the body of the fan to the northwest and the source drainage basin to the southeast. Also shown are the Coyote Hills, which serve as a barrier to fluid flow and sediment transport.

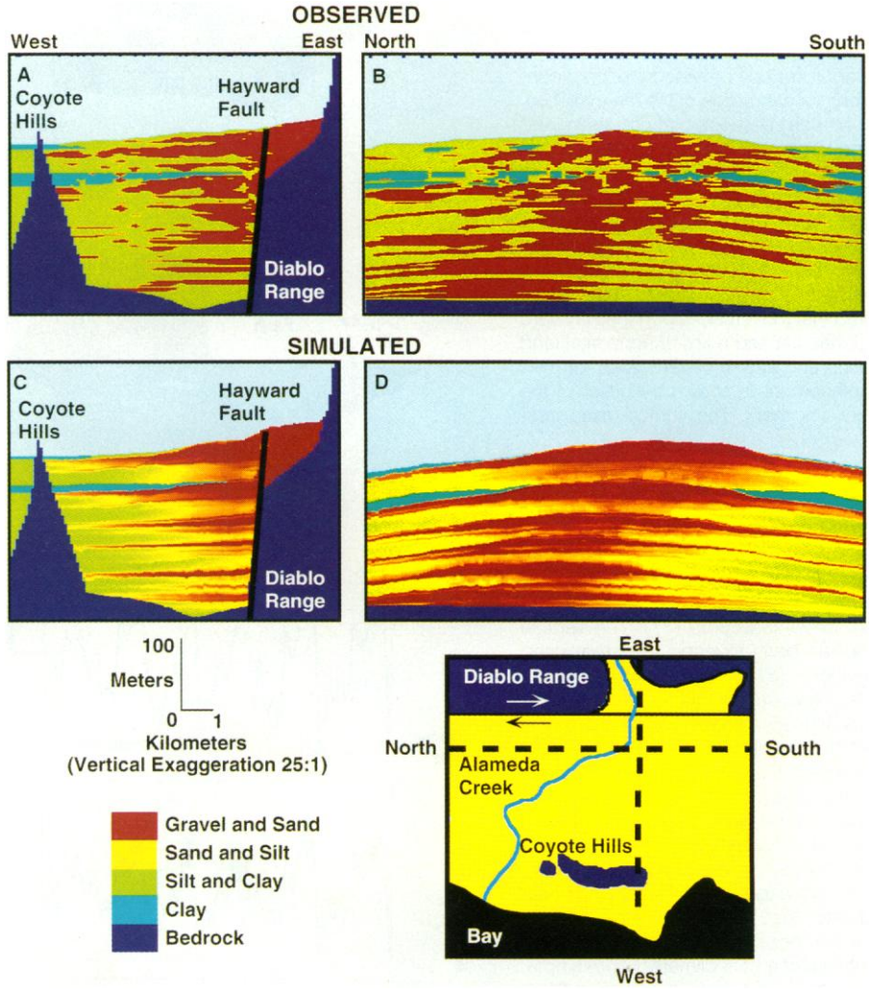

Fig. 3. Observed and simulated geologic cross sections. (**A**) and (**C**) are perpendicular to the Hayward fault, whereas (**B**) and (**D**) are parallel to the Hayward fault. Geologic data are presented from 63 water wells and bridge borings in the Alameda Creek fan (19, 21). Well and boring locations are indicated by tick marks at the tops of (A) and (B). Shown are the Hayward fault and the Coyote Hills barrier. The key sedimentary feature is the vertical cyclicity of coarse gravel and sand versus that of fine silt and clay. Estuarine deposits, which are indicated by shells and reduced clay layers, are colored blue. Simulated cross sections were based on geologic and hydrologic processes that have occurred during the past 600,000 years. The cyclicity in coarse-grained deposits is primarily a result of variations in stream flows and sediment loads. Simulation provides evidence that paleoclimatic variations during the late Quaternary were responsible for the interleaving of coarse and fine deposits. Deposition of coarse materials occurs during cooler, wetter periods, and deposition of fine materials occurs during warmer, drier periods.

least a regional control on sedimentation.

Thus, with all these factors considered, the critical question that we addressed with our model was: What were the impacts of tectonics and climate on sedimentary architecture?

Estimation of Model Parameters

We divided the modeling process into a calibration phase of 150,000 years and a simulation phase of 450,000 years. Simulation of physical processes over geologic time involves numerous model parameters and driving functions. These range from the history of past climate change to the geometry of the ancient landscape and fall into four categories: paleogeography, paleoclimate, paleohydrology, and paleosediment discharge. To avoid unconstrained estimates of numerous parameters during the calibration phase, we independently established and fixed all but six model inputs. Three of the parameter values related to flow and sediment transport dynamics. During calibration, we estimated these three values by repeatedly simulating the first 150,000 years (600,000 to 450,000 years ago) and matching the results to the observed lithology in the deeper portion of the fan. Similarly, a fourth parameter, the rate of horizontal fault motion, was estimated on the basis of a match to the deep alluvial stratigraphy during simulation of the first 150,000 years. During the simulation of the remaining 450,000 years, these four values were held constant. Finally, an additional 20,000-year calibration period was needed to estimate two model inputs controlling subaqueous deposition during high sea level 130,000 to 110,000 years ago. These two parameters were the height of sea level and the effective friction factor between freshwater and seawater.

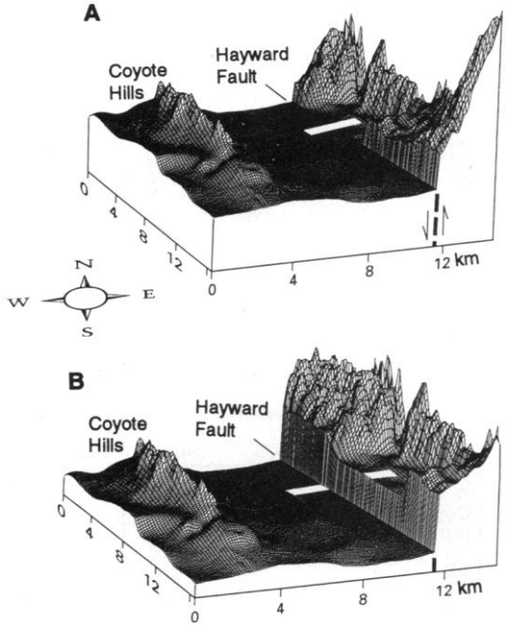

Fig. 4. Bedrock topography reconstruction. (**A**) Ancient bedrock platform as it existed 600,000 years ago before fan deposition. This platform is essentially the modern bedrock surface with the sediment stripped off and adjusted for vertical and horizontal fault motion. This bedrock surface provided the initial conditions for simulation of the fan evolution. (**B**) Modern bedrock platform estimated from geologic and geophysical data. The Coyote Hills, shown in the westerly portion of both figures, are almost entirely buried in sediment. They have served as a barrier to streamflow and sediment transport for over half a million years. In a comparison of (A) and (B), it should be noted that movement along the Hayward fault has caused 6 km of horizontal land motion and 225 m of vertical offset. This displacement is shown by offset of the white tick mark. The vertical exaggeration is ×12.

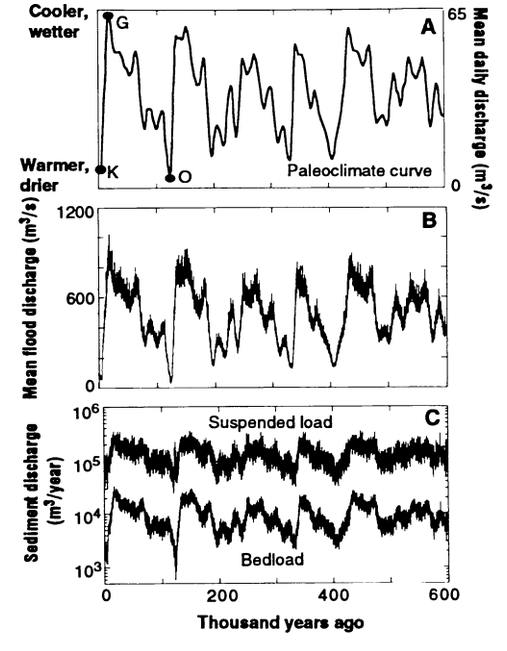

Fig. 5. (**A**) Paleoclimate curve. This relation is based on oxygen isotope data from deep-sea cores (*31*). The vertical axis has been inverted from that used previously (*31*). The vertical scale indicates that during glacial periods (the peaks) the climate was cooler and wetter and that during interglacial periods (the troughs) it was warmer and drier. Using the data from modern California Coast Range basins, we converted the global paleoclimate curve into a local paleoclimate curve applicable to the Alameda Creek drainage basin. The labeled dots indicate the basins in the California Coast Ranges that we treated as representative of a past climate. For example, the climate in Basin G, the Russian River watershed, was assumed to be analogous to the climate 20,000 years ago in the Alameda Creek basin. K, Alameda Creek basin; O, Santa Clara basin. (**B**) Average flood magnitude and (**C**) bedload and suspended load source curves. For (B) and (C), flood magnitude and source sediment were averaged over 100-year intervals. During simulations, the flood characteristics and flow versus sediment relationships varied with changing climate. The tremendous variability in the sediment source function cannot be accounted for by the paleoclimate (mean discharge) curve alone.

Paleogeography. We used sedimentary basin analysis techniques together with bedrock geometry to estimate the ancient topography 600,000 years ago. The reconstruction (Fig. 4, A and B) suggests that there have been two major changes in bedrock topography. First, approximately 225 m of vertical offset along the Hayward fault was caused by a downdropping of the San Francisco Bay block. Second, right-lateral, strike-slip motion on the Hayward fault produced approximately 6 km of horizontal offset.

Data from 24 deep water wells and limited geophysical surveys (seismic refraction, gravity, and magnetic) defined the modern bedrock topography (*20, 21, 26*). Simulation of a horizontal displacement of 1 cm per year, close to the geodetic average, was required to match deep, coarse deposits on the northwest side of the fan. The vertical displacement of the bedrock platform was estimated by realignment of both sides across the Hayward fault after a horizontal translation.

During simulations, the model kept track of paleogeographic changes and deposited sediment on top of a continuously moving platform. The rates of horizontal and vertical fault motion were held constant during the simulation. In addition, it was necessary to distinguish among the rates of subsidence that resulted from tectonics, sediment loading, and compaction. To estimate these rates, we analyzed the fan with a technique known as backstripping, in which older and older sediment layers are sequentially peeled off (*27*). Tectonic subsidence accounts for more than 70% of the total bedrock subsidence.

Paleoclimate and paleohydrology. Flooding is the primary agent of erosion, transport, and deposition in the Alameda Creek alluvial fan. The model requires a reconstructed record of individual floods over the past 600,000 years; such a record requires prediction of how climatic change has affected local hydrology.

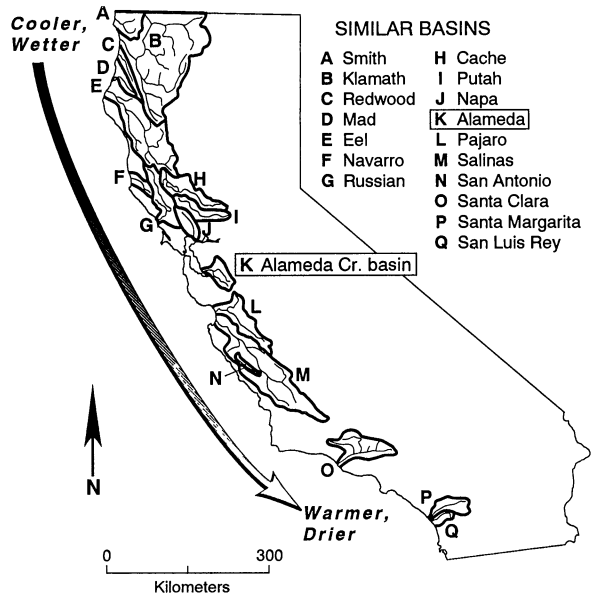

Fig. 6. California map showing drainage basins used in our analysis. The climate and hydrology of 17 drainage basins and their streams, labeled A through Q, in the California Coast Ranges were analyzed. The climate varies from cooler and wetter in the north to warmer and drier in the south. These basins were used to deduce the late Quaternary climatic history of the Alameda Creek drainage basin by a consideration of the relation of each basin to the atmospheric jet stream along with analysis of temperature- and precipitation-sensitive fossil plants and pollen. The jet stream shifted north and south along the California Coast during the Quaternary, thereby causing dramatic climate changes.

Earlier work on Quaternary paleohydrology has focused either on shifts in mean annual climate variables, such as precipitation and temperature (*28*), or on the ability of flow to transport sediment (*14*, *29*). This work provides important means to estimate the effects of climatic shifts on paleohydrology. However, such techniques do not provide a quantitative relation between flood events and climate change nor do they estimate the frequency distribution of paleofloods.

For our simulation, it was necessary to develop a relation between flood magnitude and climatic variation along the California coast. The procedure we followed relied on two important premises. First, we assumed that the global marine record of climate change could be used to represent local paleoclimatic trends. Second, we hypothesized that spatial differences in modern climate zones along the California coast serve as a surrogate for temporal shifts in local paleoclimate. By combining the long-term global trend with hydrologic data from modern basins, we estimated the 600,000-year paleoflood record of Alameda Creek.

For simulation, we needed a continuous record of late Quaternary climatic variation. Marine sediment sequences provide such information and are generally easier to interpret and more complete than the history contained in terrestrial glacial-interglacial stratigraphy (*30*). Paleoclimate trends in our model follow a smoothed curve developed from oxygen isotope data in five deep-sea cores (Fig. 5A) (*31*, *32*).

The marine record shows distinct cycles that regionally reflect cooler, wetter glacial periods and warmer, drier interglacial periods. Oak and pine pollen remains from Clear Lake, California (170 km north of the study area) (*33*), provide a 130,000-year record that correlates well with the marine oxygen-isotope record. Interglacial periods contained abundant oak, suggesting warmer and drier climatic conditions, whereas glacial periods contained abundant pine and a scarcity of oak, suggesting cooler and wetter climatic conditions. Although these climatic and floral transitions characterize the central coast of California, patterns of paleoclimate were different elsewhere (*34*, *35*).

Although the ocean record indicates climatic trends, information from modern basins is needed to estimate the paleohydrology of the Alameda Creek basin. We adopted a space-for-time analogy in which the climates of modern California coastal basins corresponded to those of our basin in the geologic past. Seventeen drainage basins in the California Coast Range were used (Fig. 6); those to the north of Alameda Creek have climates that are cooler and wetter than that of the Alameda Creek basin, whereas basins to the south are warmer and drier (*36*). Runoff is the hydrologic response to climate, expressed as a depth of water over a drainage basin (Fig. 7). We computed the statistics of streamflow, such as mean and variance, that describe runoff from these modern basins and used these values to represent specific climate conditions of the past in the

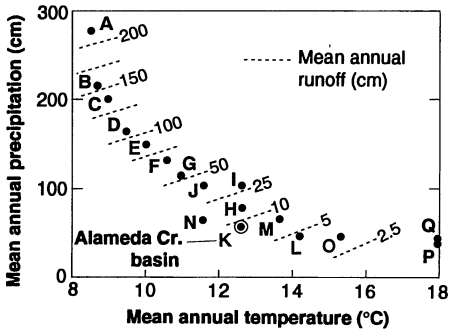

Fig. 7. Mean annual precipitation versus mean annual temperature (*36*). This relation was developed from an analysis of the 17 basins in the California Coast Ranges, labeled A through Q (as in Fig. 6). Basins in northern California are cooler and wetter, whereas those in southern California are warmer and drier. Of key importance is the dramatic trend in mean annual runoff, indicated by the dashed lines, ranging from more than 200 cm in northern California to less than 2 cm in southern California. Runoff drives sedimentation and erosion over geologic time. Climatic shifts were represented by considering the runoff and flood characteristics in the modern basins.

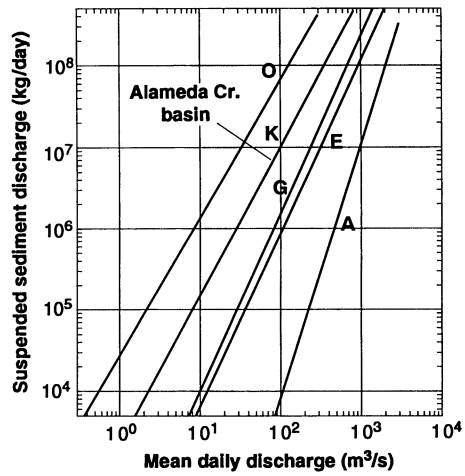

Fig. 8. Stream discharge versus suspended sediment load. In sedimentary process simulation, it is necessary to identify trends in the effects of climatic variation on sediment discharge. Each line represents a linear fit of between 1000 and 5000 daily streamflow and sediment load measurements from a particular stream, labeled as letters (as in Fig. 6). The area of each of the drainage basins represented is within 90% of the Alameda Creek basin area (K). The warmer, drier climates plot to the left of the diagram, whereas the cooler, wetter climates plot progressively to the right. Sediment data were available for 12 of the 17 basins, and all 12 basins showed this trend. In our simulation, the first step was to determine the relation between sediment discharge and enhanced streamflow that occurred during cooler and wetter periods. Basins in northern California, such as Basin A, exhibit a lower suspended sediment concentration for a given streamflow magnitude than do those in southern California, such as Basin O. The effects of basin size, slope, geology, uplift rate, and climate were analyzed, and the climate effect was dominant. Particle size data for Alameda Creek and Coast Range streams provided the basis for dividing total bedload and suspended load into component loads of gravel, sand, silt, and clay (*45*). In our model, the relation between stream discharge and total bedload is similar to the relation shown for discharge versus total suspended load, although bedload varies with the flood magnitude alone.

Alameda Creek basin (Fig. 5A). Thus, we used streamflow statistics of modern Alameda Creek, before regulation by reservoirs, for the modern climate. For warmer, drier paleoclimate conditions, the streamflow statistics of a modern basin in southern California were used. Similarly, for cooler, wetter paleoclimate conditions, the streamflow statistics of a modern basin in northern California were used. For interim periods, the flow statistics that describe paleohydrology were linearly interpolated between climate classes. With this approach, qualitative paleoclimate variations were transformed into a quantitative measure of the local paleohydrologic record (Fig. 5B).

Dated fossil plant and pollen remains were of value in guiding our association of a specific modern basin with a particular past climate regime in the Alameda Creek basin. Diagnostic fossil plant assemblages are available in the San Francisco Bay area, and flora with radiocarbon dates of 20,820 to 23,000 years ago suggest that the local climate was cooler and wetter during that glacial period (*19, 37*). At that time, incense cedar, Douglas fir, cypress, and pine were abundant, and oak and redwood were nearly absent. Today, Basin G (Fig. 6) in northern California contains a similar floral assemblage (*38*) and was chosen to represent the Alameda Creek basin during glacial conditions. Basin G is in an orographic position similar to that of the Alameda Creek basin.

We associated Alameda Creek during warmer and drier periods with modern hydrologic conditions in southern California. In the San Francisco Bay area, there was probably an abundance of oak relative to pine during the last interglacial period. We based this observation on the high oak to pine pollen ratios from Clear Lake, California, during the last interglacial period (*33*). Today, Basin O contains abundant oak and little pine and was chosen to represent our basin during interglacial conditions. In addition, during the last interglacial there were greater salinities in Bay Area estuarine deposits than there are at the present time (*39*), indicating diminished runoff and reduced freshwater inflows, just as in Basin O today (*40*).

Our ability to associate a modern coastal basin with climate conditions of the past implies that climate zones have shifted from north to south during the late Quaternary. Two lines of evidence support this. First, results from general circulation models applied to glacial and interglacial conditions indicate that the jet stream over North America underwent latitudinal shifts (*34, 41*). These shifts displaced the climate zones from north to south along the west coast as conditions changed in the transition from full interglacial periods to full glacial periods. If this is the case, over time the proximity between the Alameda Creek basin and the average position of the jet stream exerted a strong control on local paleoclimate. Second, fossil faunal and floral assemblages suggest regional north-to-south shifts in paleoclimate. Pacific Ocean sediments contain abundant evidence of Pliocene and Pleistocene latitudinal migrations of surface isotherms in the ocean and lower atmosphere (*42*). Paleoclimatically controlled shifts in foraminifera coiling ratios from southern California indicate north-to-south climatic migrations during the Quaternary (*43*). California coastal forests also experienced latitudinal migrations during the late Quaternary (*44*).

Paleosediment loads. Each flow must be associated with a sediment load. Useful data were available from 12 of the 17 modern Coast Range basins (*45*). Total sediment load includes fine sediment transported in suspension above the stream bed and coarse bedload sediment transported on the stream bed. In our model, the sediment flux was constrained by the stream's capacity for transport and not by source availability. The sediment source function (Fig. 5C) was such that suspended load was approximately an order of magnitude greater than bedload.

There is a decrease in the concentration of suspended sediment for a given magnitude of streamflow from southern to northern California coastal basins (Fig. 8). This reflects the transition from drier to wetter climates. In an arid climate, there is sparse vegetation and a consequent increase in the erosive power of flash floods. In contrast, in wetter climates a flood carries less sediment than it would in an arid climate, but of course in wetter regions there are far more floods of large magnitude that move a greater total volume of sediment (Fig. 5C).

Climate affects suspended sediment availability by influencing runoff, soil moisture content, surface cover, mineral weathering, drainage density, and storm patterns (*46*). The prevalence of landslides also contributes to the concentration of suspended sediment in streams. An increase in the relative amount of carried detritus from southern to northern California coastal streams may be partially attributed to a greater occurrence of landslides in northern California.

Data on bedload versus discharge for Coast Range streams are limited (*45*). Thus, we were unable to distinguish the effects of climate from those of basin size, slope, and geology. We therefore used a source equation for total bedload that was consistent with the limited bedload data set and that simulated the production of enough total gravel and sand to create coarse deposits attributed to Alameda Creek over the past 600,000 years. In this model, changes in the paleohydrology controlled the total bedload. For example, colder, wetter periods produced more frequent floods than warmer, drier periods, with higher discharges and velocities capable of moving more bedload material (Fig. 5C).

Results: Comparison of Simulation and Data

The geologic process simulator, together with the independently estimated paleoflood history, was used to reconstruct the evolution of the Alameda Creek fan. The simulation spanned 600,000 years, from the mid-Pleistocene uplift of the Diablo Range to the present. Comparisons were made between cross sections from the simulation and cross sections constructed from the field data. The dominant features in the simulated stratigraphy were the cycles of large wedges of gravel and sand separated by layers of silt and clay (Fig. 3C). The coarse layers thinned as they extended from the head of the fan and pinched out near the Coyote Hills.

The simulation produces a sedimentary architecture that closely resembles the real fan (Fig. 3). Its large-scale layering is the signature of paleoclimate-driven fluctuations in streamflows and sediment loads. The model yields six coarse wedges corresponding in depth and extent to the observed fan layers, with one coarse layer for each glacial cycle. Coarse layers correspond to colder, wetter periods on the paleoclimate curve, whereas fine layers correspond to warmer, drier periods. The top coarse layer corresponds to the last full glacial period, which ended 12,000 years ago, whereas the remaining five coarse layers correspond to earlier marked cold periods. The irregularity of the layers reflects variability in the paleoflood statistics and asymmetry in the transitions between climatic extremes.

Tectonic activity along the Hayward fault also left a distinct imprint in the sedimentary architecture. This appears in cross sections from field data constructed both perpendicular and parallel to the fault (Fig. 3, A and B), the trends of which occur in the simulated results (Fig. 3, C and D). Parallel to the fault (Fig. 3, B and D), there are pancake-shaped bodies of coarse material that are horizontally offset from each other. At the time of deposition, the thickest area of each pancake-shaped layer corresponded to the location of Alameda Creek. Since deposition, each ancestral deposit shifted to the north as a result of right-lateral motion along the Hayward fault. The lower left coarse pulse corresponds to the oldest cool, wet period, whereas the upper right coarse pulse corresponds to the most recent cool, wet period.

Perpendicular to the fault (Fig. 3, A and C), offset has resulted in sequentially thicker coarse wedges from the oldest and deepest deposits to the youngest and shallowest deposits. The youngest coarse sediment horizon extends further toward the bay than older, deeper horizons because over time the canyon in which Alameda Creek originates has shifted to the south and into the plane of the cross section. The lower coarse horizon was deposited at the southern margin of the ancestral fan, whereas the upper coarse horizon was deposited closer to the modern creek.

A horizontal displacement rate of 1.0 cm per year produced the best match between simulated and observed cross sections. Although this rate was calibrated for the early period 600,000 to 450,000 years ago, continued use of this average value appeared to match the spatial distribution of the coarse-grained fan deposits up to the present. Given the coarse model grid, we cannot use our estimated long-term offset rate to distinguish between seismic and aseismic displacements. Our calibrated displacement rate is at the higher end of measured values. According to geodetic measurements (47), the lateral displacement along the fault averages 1.0 to 1.2 cm per year. Holocene fault creep estimates are lower, from 0.3 to 0.9 cm per year (48).

In the simulation, high stands of relative sea level resulted in the two blue clay layers, one near the land surface and the other approximately 45 m below the land surface (Fig. 3). The lower unit was deposited 128,000 to 115,000 years ago, and the upper unit formed during the past 6,000 years. These intervals correspond to the two most recent high stands of sea level. During these times, stream gradients were low, thereby trapping stagnant water behind the Coyote Hills. In contrast, when relative sea level was low, discharge was sufficient to transport fine sediment beyond the margin of the alluvial fan and to move coarse sediment to the west around the Coyote Hills.

The height of ancestral San Francisco Bay during the last high sea level stand is uncertain. Globally, it is believed that sea level during the last interglacial period (approximately 125,000 years ago) was about 6 m above that of today (49), although estimates for this range from 2 to 10 m (50). During model experimentation, a simulated 6-m rise in the bay level was necessary to develop the continuous clay layer that extends 5 km east of the Coyote Hills at a depth of 45 m.

Conclusions

Sedimentary process simulation coupled with simulated paleoclimate-driven flood events enabled us to model the evolution of alluvial fan sediments over geologic time. Reconstruction of the Alameda Creek fan shows the relative importance of climate change, tectonics, and relative sea level change on fan formation. Simulation yields bounds on rates of fault motion and the history of relative sea level change. The alluvial deposits strongly reflect late Quaternary climatic trends that occurred in this position of the northern California Coast Ranges. Our success in matching the observed three-dimensional stratigraphy in the Alameda Creek fan with our simulated model is evidence of a genetic link between sedimentary architecture and paleoclimate. We based the record of estimated paleohydrology on an assumed similarity between the climate of modern basins and their counterparts in the geologic past. The assumed space-for-time analogy proved essential in reconstructing key features of the deposits; this approach provides reasonable constraints on paleoflood characteristics and paleosediment loads needed for process simulation.

REFERENCES AND NOTES

1. A. D. Miall, *Principles of Sedimentary Basin Analysis* (Springer-Verlag, Heidelberg, Germany, 1984); H. E. Reineck and I. B. Singh, *Depositional Sedimentary Environments* (Springer-Verlag, Heidelberg, Germany, 1980); H. Blatt, G. Middleton, R. Murray, *Origin of Sedimentary Rocks* (Prentice-Hall, Englewood Cliffs, NJ, 1980).
2. M. T. Jervey, *Soc. Econ. Paleontol. Mineral. Spec. Publ.* **42**, 47 (1988); *Kansas Geol. Surv. Sub. Geol. Ser.* **12**, 1 (1989); W. C. Pitman III, *Geol. Soc. Am. Bull.* **89**, 1389 (1978).
3. E. H. Isaaks and R. M. Srivastava, *An Introduction to Applied Geostatistics* (Oxford Univ. Press, New York, 1989); A. G. Journel and Ch. J. Huijbregts, *Mining Geostatistics* (Academic Press, London, 1978); T. A. Hewett, *Soc. Pet. Eng. J.* **15386** (1986); _____ and R. A. Behrens, *ibid.* **18326** (1988).
4. J. S. Bridge and M. R. Leeder, *Sedimentology* **26**, 617 (1979).
5. D. M. Tetzlaff and J. W. Harbaugh, *Simulating Clastic Sedimentation* (Van Nostrand Reinhold, New York, 1989); D. M. Tetzlaff, thesis, Stanford University (1987).
6. T. A. Cross, Ed., *Quantitative Dynamic Stratigraphy* (Prentice-Hall, Englewood Cliffs, NJ, 1990); P. A. Martinez and J. W. Harbaugh, in *Applications in Coastal Modeling*, C. V. Lakhan and A. S. Trenhaile, Eds. [*Elsevier Oceanogr. Ser.* **49** (1989)], pp. 297–337.
7. R. B. Bird, W. E. Stewart, E. N. Lightfoot, *Transport Phenomena* (Wiley, New York, 1960).
8. J. E. Simpson, *Gravity Currents: In the Environment and the Laboratory* (Wiley, New York, 1987).
9. A. Rachocki, *Alluvial Fans* (Wiley, New York, 1981); D. R. Spearing, *Geol. Soc. Am. Map MC-8* (1974); T. H. Nilsen and T. E. Moore, *Bibliography of Alluvial Fan Deposits* (Geo Books, Norwich, United Kingdom, 1984).
10. M. B. Fiering and B. B. Jackson, *American Geophysical Union Water Resources Monograph 1* (American Geophysical Union, Washington, DC, 1971); N. C. Matalas, *Water Resour. Res.* **3**, 937 (1967).
11. M. G. Wolman and J. P. Miller, *J. Geol.* **68**, 54 (1960).
12. E. Meyer-Peter and R. Muller, in Proceedings of the *Third Meeting of the International Association for Hydraulic Research* (Stockholm, 1948), p. 39; R. A. Bagnold, *U.S. Geol. Surv. Prof. Pap. 422-I* (1966); *Philos. Trans. R. Soc. London Ser. A* **249**, 235 (1957); M. P. DuBoys, *Ann. Ponts Chausses* **18**, 141 (1879); for a review, see V. A. Vanoni, Ed.; *Sedimentation Engineering* [*A.S.C.E. Man. Rep. Eng. Pract.* **54** (1975)].
13. I. A. Shields, *Anwendung der Ahnlichkeitsmechanik und der Turbulenzforschung auf Geschiebebewegung. Mitteilungen der Preussischen Versuchsanstalt fur Wasserbau and Schiffbau, heft 26*, W. P. Ott and J. C. van Uchelen, Transl. (Cooperative Laboratory, California Institute of Technology, Pasadena, CA, 1936); E. W. Lane and E. J. Carlson, in *Proceedings of the Minnesota International Hydraulics Convention, Joint Meeting of the International Association for Hydraulics Research and Hydraulics Division, A.S.C.E.* (Brown, Dubuque, IA, 1953), p. 37.
14. P. D. Komar, in *Flood Geomorphology*, V. R. Baker, R. C. Kochel, P. C. Patton, Eds. (Wiley, New York, 1988), pp. 97–111.
15. D. L. Turcotte and G. Schubert, *Geodynamics: Application of Continuum Physics to Geological Problems* (Wiley, New York, 1982).
16. D. Marion, thesis, Stanford University (1990).
17. Fan formation began during the last major uplift of the Diablo Range and coincident downwarping of the San Francisco Bay block (*18*). Potassium-argon dating of the Friant ash constrains the uplift date to after 615,000 years ago [D. E. Marchand and A. Allwardt, *U.S. Geol. Surv. Bull. 1470* (1981); G. H. Davis and T. B. Coplen, *Geol. Soc. Am. Spec. Pap. 234* (1989); W. R. Lettis, *U.S. Geol. Surv. Open-File Rep. 82-526* (1982)]. In the Alameda Creek watershed and on the western flanks of the Diablo Range, there are tilted and folded gravels that predate the uplift. These gravels have been dated with faunal remains at 700,000 years old [D. E. Savage, *Univ. Calif. Dept. Geol. Sci. Bull.* **28**, 215 (1951); C. Wahrhaftig and J. H. Birman, in *The Quaternary of the United States*, H. E. Wright, Jr., and D. G. Frey, Eds. (VII Congress of the International Association for Quarternary Research, Princeton Univ. Press, Princeton, NJ, 1965), pp. 299–340]. Radiometric and radiocarbon dating provides control on the age of the fan and correlative deposits. The 400,000-year-old Rockland ash bed [A. Sarna-Wojcicki, *U.S. Geol. Surv. Prof. Pap. 972* (1976); _____ *et al.*, *Quat. Res. (New York)* **23**, 236 (1985)] appears in San Francisco Bay area estuarine deposits to the north of the fan (*25*) and in backshore facies in the coastal Merced formation near San Francisco [H. E. Clifton and R. E. Hunter, in *Centennial Field Guide: Cordilleran Section* (Geological Society of America, Boulder, CO, 1987), pp. 257–262]. These deposits are correlated with San Francisco Bay estuarine deposits dated to be approximately 400,000 years old by amino acid racemization in oyster shells [B. F. Atwater, B. E. Ross, J. F. Wehmiller, *Quat. Res. (New York)* **16**, 181 (1981)] and with a thick clay layer in the Alameda Creek fan. B. F. Atwater and co-workers dated estuarine deposits from the previous high stand of sea level at 80,000 to 140,000 years old with the use of stratigraphic superposition and amino acid racemization in oyster shells. These depots are correlative throughout the San Francisco Bay area (*19, 25, 43*). Radiocarbon dates provide control on Wisconsin-age alluvial (20,000 and 23,000 years old) and eolian (less than 40,000 years old) deposits adjacent to the fan and on Holocene (less than 10,000 years old) estuarine deposits throughout the San Francisco Bay area [*19, 25, 41*; R. C. Treasher, *Calif. Div. Mines Geol. Spec. Rep.* **82**, 11 (1963)].
18. B. M. Page, *Calif. Div. Mines Geol. Bull.* **190**, 255 (1966); J. C. Branner, J. F. Newson, R. Arnold, *Santa Cruz Folio* (U.S. Geological Survey Atlas, Folio 163, Menlo Park, CA, 1909); A. C. Lawson, *Geologic Atlas of the United States No. 193: San Francisco Folio, California* (U.S. Geological Survey, Menlo Park, CA, 1914); G. D. Louderback, *Calif. Div. Mines Geol. Bull.* **154**, 75 (1951); N. L. Taliaferro, *ibid.*, p. 117; A. D. Howard, *ibid.*, p. 95; N. L. Taliaferro, *ibid.* **118**, 119 (1943).
19. B. F. Atwater, C. W. Hedel, E. J. Helley, *U.S. Geol.*

Surv. Prof. Pap. 1014 (1977).
20. *Evaluation of Ground Water Resources, South Bay, Appendix A: Geology* (California Department of Water Resources, 1967); *Calif. Dep. Water Resour. Bull. 118-1, Appendix A* (1973).
21. Alameda County Water District, CA, well logs; "Final report of preliminary soil exploration for a southern crossing of San Francisco Bay," California Department of Public Works, 1966.
22. E. J. Helley, K. R. Lajoie, W. E. Spangle, M. L. Blair, *U.S. Geol. Surv. Prof. Pap. 943* (1979).
23. K. G. Gilbert, *ibid. 105* (1917).
24. "Groundwater in the San Leandro and San Lorenzo alluvial cones of the East Bay Plain of Alameda County," Alameda County Water District, CA, 1984.
25. P. D. Trask and J. W. Rolston, *Geol. Soc. Am. Bull.* **62**, 1079 (1951).
26. E. E. Brabb and E. E. Hanna, *U.S. Geol. Surv. Geophys. Invest. Map GP-932* (1981); R. M. Hazlewood, *U.S. Geol. Surv. Misc. Field Studies Map MF-796* (1976); J. E. Taylor, thesis, Stanford University (1956).
27. J. E. VanHinte, *A.A.P.G. Bull.* **62**, 201 (1978).
28. S. A. Schumm, in *The Quaternary of the United States*, H. E. Wright and D. G. Frey, Eds. (VII Congress of the International Association for Quaternary Research, Princeton Univ. Press, Princeton, NJ, 1965), pp. 783–794; W. B. Langbein and S. A. Schumm, *Eos* **39**, 1076 (1958).
29. K. J. Gregory, Ed., *Background to Palaeohydrology* (Wiley, New York, 1983); K. J. Gregory, J. Lewin, J. B. Thornes, *Palaeohydrology in Practice: A River Basin Analysis* (Wiley, New York, 1987).
30. W. B. Harland *et al.*, *A Geologic Time Scale* (Cambridge Univ. Press, Cambridge, 1989).
31. J. Imbrie *et al.*, in *Milankovitch and Climate: Part 1*, A. L. Berger *et al.*, Eds. (Reidel, Dordrecht, The Netherlands, 1984), pp. 269–305.
32. Similar cycles in the oxygen isotope record in deep-sea cores have been analyzed [N. J. Shackleton and N. D. Opdyke, *Quat. Res.* (*New York*) **3**, 39 (1973); D. G. Martinson *et al.*, *ibid.* **27**, 1 (1987); N. G. Pisias *et al.*, *Mar. Geol.* **56**, 119 (1984)]. I. J. Winograd and co-workers developed an alternate record extending from 50,000 to 310,000 years ago on the basis of a terrestrial calcite deposit [I. J. Winograd, B. J. Szabo, T. B. Coplen, A. C. Riggs, *Science* **242**, 1275 (1988)]. Their work showed differences in the timing of key climatic events from that of the marine oxygen isotope record. Had their record been complete over the past 600,000 years, it could have been used in our study.
33. D. P. Adam, *Geol. Soc. Am. Spec. Pap.* **214**, 81 (1988); D. P. Adam and G. J. West, *Science* **219**, 168 (1983).
34. COHMAP Members, *Science* **241**, 1043 (1988).
35. F. M. Phillips *et al.*, *ibid.* **248**, 1529 (1990); G. I. Smith, *Quat. Res.* (*New York*) **22**, 1 (1984); W. G. Spaulding and L. J. Graumlich, *Nature* **320**, 441 (1986).
36. D. Hornbeck, *California Patterns: A Geographical and Historical Atlas* (Mayfield, Palo Alto, CA, 1983); W. L. Kahrl, Ed., *The California Water Atlas* (Department of Water Resources, Sacramento, CA, 1979); S. E. Rantz, *Hydrologic Investigations Atlas HA-298* (U.S. Geological Survey, Reston, VA 1968); *Water Resources Data for California Part 1: Surface Water Records* (U.S. Geological Survey, Reston, VA, 1990).
37. E. J. Helley, D. Adam, D. B. Burke, in *Progress Report on the U.S.G.S. Quaternary Studies in the San Francisco Bay Area: A Guidebook for the Friends of the Pleistocene*, V. A. Frizzell, Ed. (U.S. Geological Survey, Menlo Park, CA, 1972), pp. 19–30.
38. J. R. Griffin and W. B. Critchfield, *USDA Forest Service Res. Pap. PSW-82/1972* (1972).
39. D. Sloan, *Geol. Soc. Am. Bull.* **104**, 716 (1992).
40. Greater salinities during high stands of sea level are also caused by a greater volume of ocean water in San Francisco Bay relative to the volume of freshwater inflow (*39*).
41. CLIMAP Project Members, *Science* **191**, 1131 (1976); J. E. Kutzbach and H. E. Wright, Jr., *Quat. Sci. Rev.* **4**, 147 (1985).
42. J. C. Ingle, Jr., *G. Geol. Ser. 22* **XLI**, fasc. I-II, 359 (1977).
43. M. B. Lagoe and P. R. Thompson, *J. Foraminiferal Res.* **18**, 250 (1988).
44. D. I. Axelrod, in *Terrestrial Vegetation of California*, M. G. Balbour, and J. Major, Eds. (California Native Plant Society Special Publication No. 9, Wiley, New York, 1988), pp. 139–194.
45. *Water Resources Data for California Part 2: Water Quality Records* (U.S. Geological Survey, Reston, VA, 1990); G. P. Williams and D. R. Rosgen, *U.S. Geol. Surv. Open-File Rep. 89-67* (1989).
46. D. F. Ritter, *Process Geomorphology* (Brown, New York, 1986); S. A. Schumm, *The Fluvial System* (Wiley, New York, 1977).
47. G. Borchardt, J. J. Lienkaemper, J. F. Wilmesher, *California Geol.* **43**, 36 (1990).
48. J. J. Lienkaemper, G. Borchardt, M. Lisowski, *J. Geophys. Res.* **96**, 18261 (1991); R. Nason, *Cal. Div. Mines Geol. Spec. Publ.* **62**, 22 (1982); W. H. Prescott and M. Lisowski, *ibid.*, p. 231; ———, J. C. Savage, *J. Geophys. Res.* **86**, 10853 (1981).
49. CLIMAP Project Members, *Quat. Res.* (*New York*) **21**, 123 (1984); B. J. Szabo, J. I. Tracey, Jr., E. R. Goter, *ibid.* **23**, 54 (1985).
50. There is evidence for a stand of high sea level 125,000 years ago from 2 to 10 m above the present sea level [H. H. Veeh, *J. Geophys. Res.* **71**, 3379 (1966); J. Chappell, *Geol. Soc. Am. Bull.* **85**, 553 (1974)]. G. Valensise and S. N. Ward estimate that the sea level 125,000 years ago along the central California coast was 8.9 ± 3 m higher than today [G. Valensise and S. N. Ward, *Bull. Seismol. Soc. Am.* **81**, 1694 (1991)]. They compared uplift on the Loma Prieta fault plane of the San Andreas fault to California coastal marine terrace deposits. Estuarine microfossils in San Francisco Bay area deposits to the north of the study region indicate that the bay level 125,000 years ago may have been at least 6 m higher than today and that the shore line was at least 4.8 km inland of the present shore line (*39*).
51. We gratefully acknowledge the National Science Foundation Earth Science Division (grant numbers EAR-8903631 and EAR-9118400) for funding this work. We are grateful to IBM, the office of Academic Information Resources at Stanford, and R. Street for providing supercomputer time on the IBM3090 on the Stanford campus. We also are most appreciative of the Hewlett-Packard Company for its grant of computer equipment used in this work. We thank J. Harbaugh and students for their foundational contributions to sedimentary process simulation and D. Tetzlaff for original construction of the Sedsim code.